

# An Oxetane-based Polyketide Surrogate to Probe Substrate Binding in a Polyketide Synthase

Bryan D. Ellis<sup>1†</sup>, Jacob C. Milligan<sup>2†</sup>, Alexander R. White<sup>2</sup>, Vy Duong<sup>3</sup>, Pilar X. Altman<sup>2</sup>, Lina Y. Mohammed<sup>4</sup>, Matthew P. Crump<sup>4</sup>, John Crosby<sup>4</sup>, Ray Luo<sup>3</sup>, Christopher D. Vanderwal,<sup>1\*</sup> Shiou-Chuan Tsai<sup>2\*</sup>

<sup>1</sup>1102 Natural Sciences II, Department of Chemistry, University of California, Irvine, 92697-2025, USA

<sup>2</sup>2218 Natural Sciences I, Departments of Molecular Biology and Biochemistry, Chemistry, and Pharmaceutical Sciences, University of California, Irvine, CA 92697

<sup>3</sup>3206 Natural Sciences I, Departments of Molecular Biology and Biochemistry, Biomedical Engineering, and Chemical Engineering & Materials Science, University of California, Irvine, CA 92697

<sup>4</sup>School of Chemistry, University of Bristol, United Kingdom, Bristol BS8 1TS, United Kingdom.

## Supporting Information

### Table of Contents:

#### Experimental Information:

I.	Materials and Methods.....	S1
II.	List of Abbreviations.....	S1
III.	Experimental Procedures and Characterization Data.....	S2
IV.	Expression, Purification, and Crystallization of DpsC.....	S5
V.	X-Ray Crystallographic Collection and Refinement Data.....	S6

<b>Molecular Dynamic (MD) Simulations.....</b>	<b>S6</b>
--	-----------

<b>SI References.....</b>	<b>S8</b>
---------------------------	-----------

<b>SI Tables.....</b>	<b>S10</b>
-----------------------	------------

Table S1. Statistics of Data Collection, Processing and Refinement.....	S10
---	-----

Table S2. DpsC & Ligand Simulation Conditions.....	S11
--	-----

Table S3. MM/PBSA-derived $\Delta G$ Relative Binding Free Energy Approximations.....	S11
---	-----

<b>SI Figures.....</b>	<b>S12</b>
------------------------	------------

Figure S1. Ligand-free and ligand-bound structural comparison.....	S12
--	-----

Figure S2. DpsC active site pocket.....	S13
---	-----

Figure S3. SA-Omit $ 2F_o - F_c $ map for <b>1</b> .....	S13
--	-----

Figure S4. Proposed DpsC oxyanion hole.....	S14
---	-----

Figure S5. Backbone RMSD of 100-ns simulations.....	S15
---	-----

Figure S6. Convergence trend lines of average $\Delta G$ binding energy calculations.....	S16
---	-----

Figure S7. Heavy-atom RMSF of all DpsC-malonate simulations.....	S17
--	-----

Figure S8. Heavy-atom (C, C $\alpha$ , N, O) RMSF of all DpsC-oxetane simulations.....	S18
--	-----

Figure S9. Average backbone (C, C $\alpha$ , N, O) RMSF.....	S19
--	-----

Figure S10. Alignment of mean simulated structures.....	S20
---	-----

**I. Materials and Methods.**

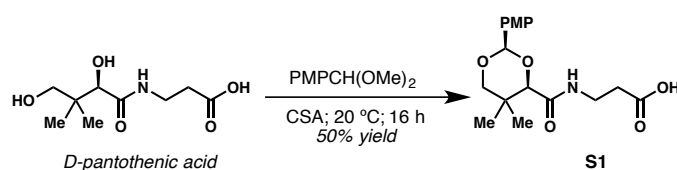
All reactions were carried out in flame- or oven-dried glassware under a positive pressure of argon (Ar), unless otherwise noted. Dry acetonitrile (MeCN), dichloromethane (CH<sub>2</sub>Cl<sub>2</sub>), diethyl ether (Et<sub>2</sub>O), tetrahydrofuran (THF), and dimethylformamide (DMF) were obtained by passage of the solvents through a column of neutral alumina under an atmosphere of argon. No precautions were made towards extruding air in aqueous media, unless otherwise noted. Solvents used for workup and chromatography such as CH<sub>2</sub>Cl<sub>2</sub>, ethyl acetate (EtOAc), hexanes, pentanes, and methanol were used as received from their respective suppliers. Reagents were used as received by their respective suppliers unless otherwise noted. Reactions were monitored by analytical thin-layer chromatography (TLC) using Merck 60 F<sub>254</sub> glass-backed silica gel (SiO<sub>2</sub>) TLC plates. TLC plates were visualized with UV irradiation (254 nm) and treatment with *p*-anisaldehyde or KMnO<sub>4</sub>/H<sub>2</sub>SO<sub>4</sub>. Flash chromatography was performed on EMD 60 Å (40–63 μm) mesh SiO<sub>2</sub>. NMR spectra were collected on Bruker GN500, CRYO500, or AVANCE600 instruments. <sup>1</sup>H and <sup>13</sup>C NMR spectra are referenced using the signal(s) of the residual undeuterated solvent. All spectra were collected at 298 K, unless otherwise indicated. Chemical shifts are reported in parts per million (ppm) and multiplicities are abbreviated as follows: s (singlet), d (doublet), t (triplet), q (quartet), quin (quintet), sept (septet), m (multiplet), br (broad), ap (apparent). Coupling constants (*J*) are reported in Hertz (Hz). Infrared (IR) spectra were collected on a Varian 640-IR spectrometer and peaks are recorded in cm<sup>-1</sup>. High resolution mass spectra (HRMS) were obtained using a Walters LCT Premier spectrometer using electrospray ionization-time of flight (ESI) or chemical ionization-time of flight (CI).

**II. List of Abbreviations**

AcOH	acetic acid
ADP	adenosine diphosphate
ATP	adenosine triphosphate
CDI	1,1'-carbonyldiimidazole
CSA	10-camphorsulfonic acid
DBU	1,8-diazabicyclo[5.4.0]undec-7-ene

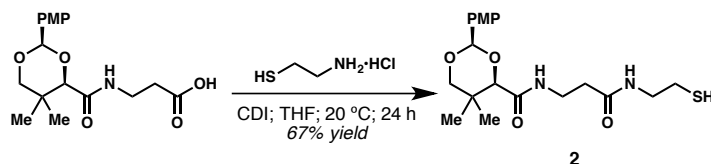
Et <sub>2</sub> O	diethyl ether
EtOAc	ethyl acetate
LRMS	low resolution mass spectrometry
MeCN	acetonitrile
MeOH	methanol
PMP	<i>p</i> -methoxyphenyl
THF	tetrahydrofuran

### III. Experimental Procedures and Characterization Data



#### PMP-Protected Pantetheine Acid S1.

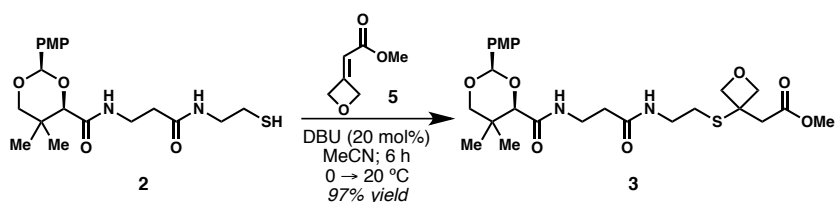
PMP-protection of *D*-pantothenic acid was performed as described by Burkart *et al.*<sup>1</sup> The spectroscopic data are consistent with previously reported data.<sup>1-2</sup>



#### PMP-Protected Pantetheine Thiol 2.

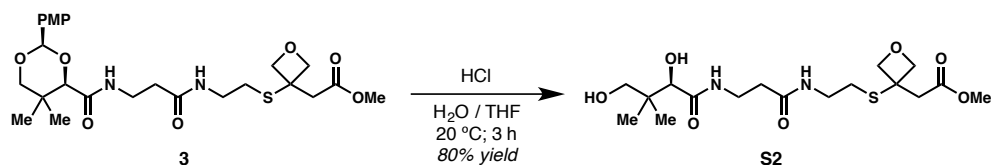
CDI (72 mg, 0.45 mmol) was added in one aliquot to a stirring solution of PMP-protected acid **S1** (100 mg, 0.30 mmol) in 2 mL THF. Cysteamine-HCl (50 mg, 0.45 mmol) was added in one portion to the vigorously stirring reaction mixture 1 h after the complete dissolution of solids. After 24 h at ambient temperature, the solvent was removed *in vacuo* and the resultant viscous oil was suspended in CH<sub>2</sub>Cl<sub>2</sub> (10 mL). The crude mixture was partitioned with an equivalent volume of sat. aq. NH<sub>4</sub>Cl, and the aqueous layer was further extracted with CH<sub>2</sub>Cl<sub>2</sub> (2 × 10 mL). The organic layers were combined, washed with brine (1 × 10 mL), dried over Na<sub>2</sub>SO<sub>4</sub>, filtered, and concentrated *in vacuo*. The amber residue was purified by flash column chromatography (SiO<sub>2</sub>, 100% EtOAc + 1% v/v AcOH) to yield the desired thiol **2** (78 mg, 67%) as a pale yellow oil. <sup>1</sup>H NMR (500 MHz, CDCl<sub>3</sub>) δ 7.40 (d, *J* = 8.4 Hz, 2 H), 7.01 (s, 1 H), 6.90 (d, *J* =

8.4 Hz, 2 H), 6.45 (s, 1 H), 5.44 (s, 1 H), 4.06 (s, 1 H), 3.80 (s, 3 H), 3.65 (q,  $J = 11.3$  Hz, 2 H), 3.55–3.51 (m, 2 H), 3.39 (ddd,  $J = 26.5, 13.5, 6.7$  Hz, 1 H), 3.33 (ddd,  $J = 26.0, 13.1, 6.1$  Hz, 1 H), 2.57 (ap dd,  $J = 14.8, 7.3$  Hz, 2 H), 2.41 (t,  $J = 6.5$  Hz, 2 H), 1.33 (t,  $J = 8.3$  Hz, 1 H), 1.07 (d,  $J = 7.6$  Hz, 6 H);  $^{13}\text{C}$  NMR (125 MHz,  $\text{CDCl}_3$ )  $\delta$  170.9, 169.5, 160.2, 130.0, 127.4, 113.7, 101.3, 83.7, 78.3, 55.3, 42.3, 35.9, 34.8, 33.0, 24.4, 21.8, 19.1; IR (thin film) 3318, 2957, 1660, 1615, 1519, 1461, 1391, 1249, 1103, 1031, 832, 731  $\text{cm}^{-1}$ ; HRMS (ESI)  $m/z$  calcd for  $\text{C}_{19}\text{H}_{28}\text{N}_2\text{O}_5\text{SNa}$   $[\text{M} + \text{Na}]^+$  419.1617, found 419.1630.



### PMP-Protected Pantetheine Ester 3.

To a solution of PMP-protected thiol **2** (421 mg, 1.06 mmol) in 4 mL MeCN at 0 °C was added methyl enoate **5** (150 mg, 1.2 mmol) in 2 mL MeCN. The reaction mixture was sparged for 5 min via the passage of Ar through the solution. Upon removing the sparging needle, DBU (30  $\mu\text{L}$ , 0.19 mmol) was added in one aliquot. The pale yellow solution was warmed to ambient temperature and allowed to stir for 6 h. The reaction mixture was then concentrated to approximately 2 mL *in vacuo* and purified by flash column chromatography ( $\text{SiO}_2$ , 0  $\rightarrow$  10% MeOH in EtOAc) to give the title compound (540 mg, 97% yield).  $^1\text{H}$  NMR (500 MHz,  $\text{CDCl}_3$ )  $\delta$  7.42 (d,  $J = 8.5$  Hz, 2 H), 7.03 (s, 1 H), 6.91 (d,  $J = 8.5$  Hz, 2 H), 6.40 (s, 1 H), 5.45 (s, 1 H), 4.75 (dd,  $J = 4.7, 2.5$  Hz, 2 H), 4.63 (dd,  $J = 6.9, 3.6$  Hz, 2 H), 4.08 (s, 1 H), 3.82 (s, 3 H), 3.68 (s, 3 H and q,  $J = 11.9$  Hz, 2 H), 3.59–3.48 (m, 2 H), 3.41 (ddd,  $J = 13.2, 6.6$  Hz, 1 H), 3.37 (ddd,  $J = 26.4, 13.0, 6.2$  Hz, 1 H), 2.98 (s, 2 H), 2.73 (t,  $J = 6.6$  Hz, 2 H), 2.44 (t,  $J = 6.3$  Hz, 2 H), 1.08 (d,  $J = 3.9$  Hz, 6 H);  $^{13}\text{C}$  NMR (125 MHz,  $\text{CDCl}_3$ )  $\delta$  171.0, 170.3, 169.5, 160.2, 130.2, 127.5, 113.7, 101.3, 83.8, 81.9, 78.5, 55.3, 51.9, 47.1, 42.4, 39.1, 35.9, 34.7, 33.1, 29.0, 21.8, 19.1; IR (thin film) 2952, 1735, 1663, 1519, 1249, 1103, 1030, 833  $\text{cm}^{-1}$ ; HRMS (ESI)  $m/z$  calcd for  $\text{C}_{25}\text{H}_{36}\text{N}_2\text{O}_8\text{SNa}$   $[\text{M} + \text{Na}]^+$  547.2090, found 547.2080.



### Pantetheine Methyl Ester **S2**.

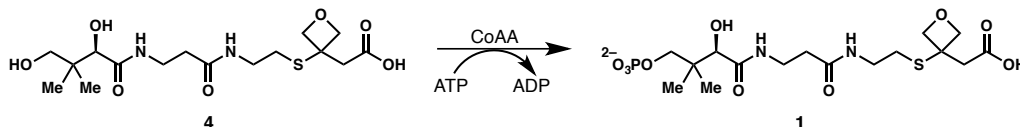
Aqueous HCl (2 mL, 1 N) was added to a stirring solution of PMP-protected methyl ester **3** (100 mg, 0.19 mmol) in 2 mL THF. The solution was allowed to stir at ambient temperature until TLC indicated the complete consumption of starting material (3 h). Saturated aqueous NaHCO<sub>3</sub> (4 mL) was then added in one aliquot to neutralize the solution. The solvent was removed by passing N<sub>2</sub> gently over the vigorously stirring solution for 13 h. The beige salts were taken up in approximately 50 mL of 20% MeOH in CH<sub>2</sub>Cl<sub>2</sub>, sonicated to break up the solids, filtered, and concentrated *in vacuo* to yield the deprotected methyl ester **4** (80 mg, 80%) as a white solid. The crude methyl ester was used directly in the next step below without further purification. <sup>1</sup>H NMR (400 MHz, D<sub>2</sub>O) δ 4.93 (d, *J* = 7.0 Hz, 2 H), 4.65 (d, *J* = 7.0 Hz, 2 H), 4.00 (s, 1 H), 3.73 (s, 3 H), 3.45–3.57 (m, 3 H), 3.35–3.43 (m, 3 H), 3.16 (s, 2 H), 2.82 (t, *J* = 6.4 Hz, 2 H), 2.50 (t, *J* = 5.4 Hz, 2 H), 0.93 (s, 3 H), 0.89 (s, 3 H); <sup>13</sup>C NMR (125 MHz, CDCl<sub>3</sub>) δ 175.2, 174.1, 173.0, 82.2, 75.9, 68.5, 52.4, 46.7, 41.4, 39.0, 38.7, 35.6, 35.3, 28.2, 20.6, 19.2; HRMS (ES) *m/z* calcd for C<sub>17</sub>H<sub>30</sub>N<sub>2</sub>O<sub>7</sub>SNa [M + Na]<sup>+</sup> 429.1671, found 429.1660.



### Pantetheine Carboxylic Acid **4**.

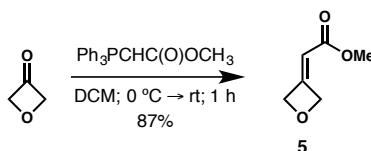
Aqueous LiOH·H<sub>2</sub>O (2 mL, 1 N) was added to a stirring solution of pantetheine methyl ester **S2** (80 mg, 0.20 mmol) in a 2:1 mixture of THF/H<sub>2</sub>O (8 mL). The mixture was stirred at ambient temperature until TLC indicated complete consumption of starting material (30 min), upon which saturated aqueous NaHCO<sub>3</sub> (4 mL) was added in one aliquot. The crude reaction mixture was concentrated by gently passing N<sub>2</sub> over the vigorously stirring solution for 16 h. The white salts were suspended in approximately 30 mL of MeOH and sonicated to break up most of the solids. The slurry was then filtered and concentrated *in vacuo*, affording the title

compound (70 mg, 90% yield) as a white solid. No further purification was used prior to the next reaction (below).  $^1\text{H}$  NMR (500 MHz,  $\text{D}_2\text{O}$ )  $\delta$  4.94 (d,  $J = 7.4$  Hz, 2 H), 4.64 (d,  $J = 7.4$  Hz, 2 H), 4.00 (s, 1 H), 3.55–3.51 (m, 3 H), 3.42 (t,  $J = 6.7$  Hz, 2 H and d,  $J = 11.7$  Hz, 1 H), 3.39 (s, 1 H), 2.85 (s, 2 H and t,  $J = 6.7$  Hz, 2 H), 2.52 (t,  $J = 6.4$  Hz, 2 H), 0.93 (s, 3 H), 0.90 (s, 3 H);  $^{13}\text{C}$  NMR (125 MHz,  $\text{CD}_3\text{OD}$ )  $\delta$  178.1, 176.1, 173.8, 83.9, 77.2, 70.3, 49.9, 46.9, 40.6, 40.4, 36.4, 36.3, 29.5, 21.4, 21.0; HRMS (ESI)  $m/z$  calcd for  $\text{C}_{16}\text{H}_{28}\text{N}_2\text{O}_7\text{SNa}$   $[\text{M} + \text{Na}]^+$  415.1515, found 415.1522.



### Malonate Mimic 1.

A buffer solution of potassium phosphate (25 mM, pH 7.5, 93  $\mu\text{L}$  total volume), 1 M  $\text{MgCl}_2$  (1  $\mu\text{L}$ , 10 mM), 500 mM ATP- $\text{K}_2$  salt (1.6  $\mu\text{L}$ , 8 mM), 57  $\mu\text{M}$  CoAA (1.75  $\mu\text{L}$ , 1  $\mu\text{M}$ ), 100 mM **4** in DMSO (2.5  $\mu\text{L}$ , 2.5 mM) were added to an Eppendorf tube and homogenized with a vortex mixer. The reaction was incubated at 37  $^\circ\text{C}$  for 90 min, upon which it was filtered using a Pierce<sup>TM</sup> Protein Concentrator (PES 3K WMC0). The solution was then injected into an HPLC column (Beckman Coulter<sup>TM</sup> Ultrasphere ODS, 5  $\mu$  particle size, 10 mm x 15 cm) and eluted with  $\text{MeCN} + 0.1\%$  v/v formic acid in  $\text{H}_2\text{O} + 0.1\%$  v/v (gradient elution: 5%  $\rightarrow$  95%). Fractions were analyzed using LRMS (ES) and the fractions containing product with the least ATP / ADP were pooled, concentrated under a stream of  $\text{N}_2$ , and used in the co-crystallographic studies without further purification. HRMS (ES)  $m/z$  calcd for  $\text{C}_{16}\text{H}_{28}\text{N}_2\text{O}_{10}\text{PS}$   $[\text{M} + \text{H}]^-$  471.1202, found 471.1208.



### Methyl 2-(oxetan-3-ylidene)acetate (5).

*Note: Methyl enoate 5 was prepared by modification of the procedure of Wuitschik.<sup>3</sup>*

A solution of 3-oxetanone (200 mg, 2.8 mmol) in 2 mL  $\text{CH}_2\text{Cl}_2$  was cooled to 0  $^\circ\text{C}$ , upon which a solution of methyl (triphenylphosphoranylidene)acetate (1200 mg, 3.6 mmol) in 6 mL  $\text{CH}_2\text{Cl}_2$  was transferred slowly via cannulation. The flask containing the Wittig reagent was rinsed with approximately 2 mL of  $\text{CH}_2\text{Cl}_2$ , which was cannulated into the reaction flask. After

30 min at 0 °C, the flask was allowed to warm to ambient temperature. The pale yellow solution was allowed to stir for another 30 min, upon which it was poured onto a plug of silica gel and eluted with 1:1 EtOAc:hexanes. The volatiles were removed *in vacuo* yielding methyl enoate **5** (320 mg, 90% yield). <sup>1</sup>H NMR (500 MHz, CDCl<sub>3</sub>) δ 5.64 (quin, *J* = 2.4 Hz, 1 H), 5.49 (ap dd, *J* = 6.9, 3.0 Hz, 2 H), 5.29 (ap dd, *J* = 7.0, 3.7 Hz, 2 H), 3.71 (s, 3 H); <sup>13</sup>C NMR (125 MHz, CDCl<sub>3</sub>) δ 165.6, 159.1, 110.6, 81.0, 78.4, 51.4; IR (thin film) 2924, 2856, 2360, 1720, 1698, 1437, 1353, 1211, 1101, 956 cm<sup>-1</sup>; HRMS (CI) *m/z* calcd for C<sub>6</sub>H<sub>9</sub>O [M + H]<sup>+</sup> 129.0552, found 129.0550.

#### **IV. Expression and Purification of DpsC**

A pET28 expression vector coding for 6xHis-tagged DpsC was transformed into *E. coli* BL21(DE3) by heatshocking at 42 °C for 45 seconds. The transformed cells were plated on an LB medium supplemented with 50 µg/mL kanamycin and incubated at 37 °C for 18 hours. Cells were transferred to a 10 mL starter culture supplemented with 50 µg/mL kanamycin and shaken at 250 rpm for 18 hours at 37 °C. 10 mL of the starter culture was transferred to 1 L of LB media supplemented with 50 µg/mL kanamycin. The cultures were shaken at 200 rpm at 37 °C until the OD<sub>600</sub> reached 0.6; the expression was induced by addition of 1 mM IPTG, and the cultures were shaken for 18 hours at 18 °C. The cells were centrifuged for 10 minutes, resuspended in lysis buffer (50 mM Tris pH 8.0, 300 mM NaCl, 10 mM imidazole, 10% glycerol), and flash frozen in liquid nitrogen before storage at -80 °C.

The cells were lysed using a microfluidizer, and the lysate was centrifuged at 21,000 rcf for 1 hour to separate from cellular debris. The lysate was applied to a 5 mL HisTrap HP column (GE Healthcare) and eluted using an imidazole gradient via an Akta Purifier FPLC. The fractions were analyzed using SDS-PAGE, and the fractions containing DpsC were combined and concentrated to 5 mg/mL. The protein sample was further purified using a Superdex 200 column (GE Healthcare), and fractions were again analyzed using SDS-PAGE. The selected fractions containing DpsC were concentrated to 4 mg/mL and flash frozen in liquid nitrogen before storage at -80 °C.

#### **V. Crystallization and Structure Solution of the Propionyl-DpsC-probe Complex**

DpsC was crystallized in a solution containing 0.06 M MgCl<sub>2</sub>, 0.6 M CaCl<sub>2</sub>, 0.1 M imidazole pH 7.0, 0.1 M MES pH 6.7, 15% PEG 4000, and 30% Glycerol. The crystals were improved through multiple rounds of seeding using a Seed Bead (Hampton Research). The crystals were incubated in a 5 mM solution of propionyl-CoA prepared using mother liquor for 18 hours to form the propionyl-DpsC intermediate, transferred to a drop containing 5 mM **1** for 3 hours, and flash frozen in liquid nitrogen. The diffraction pattern of the crystals was measured at the Advanced Light Source using beamline 8.2.2. The diffraction images were processed using HKL2000<sup>4</sup>. The structure was solved by molecular replacement by Phaser using the *apo* DpsC structure (PDB:5TT4, submitted) as the search model<sup>5</sup>. The model was built by Coot and refined using the Phenix suite<sup>6-8</sup>. The statistics of data collection, processing and model building are listed in Table S1.

### **Molecular dynamics (MD) Simulations**

The crystal structure of DpsC bound to oxetane-based probe **1** in this study was used for parameterization and setup of MD simulations. The same topology and coordinates of this structure were adopted for the simulation of DpsC with malonyl-PPT by mutating the oxetane-substituent *in silico* into a carbonyl group using the program Chimera. The Amber ff14SB force field<sup>9-13</sup> was used to parameterize the DpsC receptor. Two non-standard residues in DpsC were parameterized using RESP ESP charge Derive Server (R.E.D.S)<sup>14-15</sup>. Both malonate- and oxetane-based ligands were then parameterized using the general Amber force field (GAFF) and ff14SB forcefields<sup>9-13</sup>.

Prior to minimization, complexes were neutralized with sixteen Na<sup>+</sup> counter-ions and solvated explicitly using a 10 Å buffer of TIP3P waters in a truncated octahedron box. Both systems underwent a two-step minimization using SANDER<sup>9-13</sup> to remove any steric clashes and overlaps. All hydrogen-containing bonds were constrained using the SHAKE algorithm<sup>16</sup>. DpsC-ligand complexes were then heated to 310K for 100-ps in the NVT ensemble, and equilibrated for 10-ns at 310K in the NPT ensemble. The accelerated CUDA version of PMEMD



was subsequently used to generate 100-ns production runs of all DpsC-ligand complexes in the NVT ensemble with 2-fs time steps.

For each of the two DpsC-ligand complexes – DpsC-malonyl-PPT and DpsC-1, three independent 100-ns trajectories were generated. A length of 100-ns for production runs is appropriate for both systems to converge at the physiological temperature. Backbone RMSD of DpsC complexes with respect to the first frame structure (Figure S5) demonstrates stability and convergence of the systems. Simulation conditions are listed in Table S2.

RMSD analysis of the two DpsC chains (chain A and chain B) in all six simulations revealed that RMSD of chain B converges to lower values (Figure S5). Given its higher stability, we then proceeded to compare the binding interactions between the malonate- and oxetane-based ligands in chain B of DpsC using the Molecular Mechanics Poisson-Boltzman Surface Area (MM/PBSA) module of Amber 16<sup>17-22</sup>. Specifically, the finite-difference Poisson Boltzmann method and the modern nonpolar solvation model were used in the solvation free energy calculation in MM/PBSA<sup>23-28</sup>. Considering the charged phosphopantetheine probes and DpsC residues, an internal protein dielectric constant of 20 was used in MM/PBSA calculations<sup>21-22</sup>. Both systems only differ with regards to a single substituent on the ligand – oxetane or carbonyl – thus *relative* binding affinity approximations are sufficient for analysis instead of *absolute* binding free energies (Table S3), which require more demanding conformational entropy calculations. Relative binding affinities were then calculated using the last 10-ns (frames 900 to 1000) of all three 100-ns production trajectories (Figure S). Convergence trend lines are provided in Figure S6, demonstrating the  $\Delta G$  of both ligands converges after 6-ns. As listed in Table S3, the binding affinities of malonate- and oxetane-based probes are within one standard deviation of another, demonstrating similar binding affinities.

Using the CPPTRAJ module of Amber 16, we then conducted root-mean-square fluctuation (RMSF) analyses of backbone atoms (C, C $\alpha$ , N, O) for all MD runs. The RMSF values provide overall movement of each residue from its mean position, revealing high-frequency motion of the protein. Loop regions and terminal sequences exhibit the highest degree of fluctuation. The average RMSF calculations of DpsC-malonate (Figure S7) and –oxetane (Figure S8) simulations are displayed. Further the average RMSF values are also visualized in the

context of the structures in Figure S9, rendered using the Chimera program. To determine long-time, overall motion of DpsC in response to either malonate- or oxetane-based ligands, the CPPTRAJ module of Amber 16 was employed once again to conduct Principal Component Analysis (PCA) and generate two movies<sup>29</sup>. PCA analysis consists of calculating a covariance matrix in which orthogonal vectors with the highest variance are selected as principal components (PCs). Using the first PC to generate movies of malonate- and oxetane-bound DpsC from DpsC-malonate simulation 1 and DpsC-oxetane simulation 5, we observe a general outward “breathing” motion exhibited by both complexes. Alpha helices 1-2 exhibit movement towards the ligand, and overall examination of PCA MD movies demonstrates minimal deviation between DpsC-malonate and DpsC-oxetane PCA movies. Figure S10 visualizes an alignment between the two snapshots closest to the mean structure (namely, with the lowest RMSD) of malonate and oxetane trajectories. Frame 337 of DpsC-malonate simulation 1 and frame 106 of DpsC-oxetane simulation 5 were chosen for alignment. The backbone (C, C $\alpha$ , N) RMSD between the two mean structures is 0.716 Å, excluding the loop regions and the terminal regions. Overall, the computational analyses mentioned here demonstrate highly similar electronic, thermodynamic, and conformational influences propagated by malonyl-PPT and oxetane-based probe **1** in DpsC.

## SI References

1. Clarke, K. M.; Mercer, A. C.; La Clair, J. J.; Burkart, M. D., *J Am Chem Soc* **2005**, *127* (32), 11234-5.
2. Shakya, G.; Rivera, H., Jr.; Lee, D. J.; Jaremko, M. J.; La Clair, J. J.; Fox, D. T.; Haushalter, R. W.; Schaub, A. J.; Bruegger, J.; Barajas, J. F.; White, A. R.; Kaur, P.; Gwozdzowski, E. R.; Wong, F.; Tsai, S. C.; Burkart, M. D., *J Am Chem Soc* **2014**, *136* (48), 16792-9.
3. Wuischik, G. Oxetanes in Drug Discovery. . ETH Zürich,, 2008.
4. Otwinowski, Z.; Minor, W., *Method Enzymol* **1997**, *276*, 307-326.
5. Mccoy, A. J.; Grosse-Kunstleve, R. W.; Adams, P. D.; Winn, M. D.; Storoni, L. C.; Read, R. J., *J Appl Crystallogr* **2007**, *40*, 658-674.
6. Emsley, P.; Cowtan, K., *Acta Crystallogr D* **2004**, *60*, 2126-2132.
7. Terwilliger, T. C.; Grosse-Kunstleve, R. W.; Afonine, P. V.; Moriarty, N. W.; Zwart, P. H.; Hung, L. W.; Read, R. J.; Adams, P. D., *Acta Crystallogr D* **2008**, *64*, 61-69.
8. Afonine, P. V.; Grosse-Kunstleve, R. W.; Echols, N.; Headd, J. J.; Moriarty, N. W.; Mustyakimov, M.; Terwilliger, T. C.; Urzhumtsev, A.; Zwart, P. H.; Adams, P. D., *Acta Crystallogr D* **2012**, *68*, 352-367.
9. Case, D. A., Darden, T., Cheatham, T.E., III, Adrian Roitberg, C.S., Wang, J., Duke, R.E., Luo, R., Roe, D.R., Walker, R.C., Legrand, S., et al. (2014b), **Amber 14 Reference Manual (University of California)**.
10. Gotz, A. W.; Williamson, M. J.; Xu, D.; Poole, D.; Le Grand, S.; Walker, R. C., *J Chem Theory Comput* **2012**, *8* (5), 1542-1555.
11. Wang, J.; Wang, W.; Kollman, P. A.; Case, D. A., *J Mol Graph Model* **2006**, *25* (2), 247-60.
12. Wang, J.; Wolf, R. M.; Caldwell, J. W.; Kollman, P. A.; Case, D. A., *J Comput Chem* **2004**, *25* (9), 1157-74.
13. Wickstrom, L.; Okur, A.; Simmerling, C., *Biophys J* **2009**, *97* (3), 853-6.
14. Dupradeau, F. Y.; Pigache, A.; Zaffran, T.; Savineau, C.; Lelong, R.; Grivel, N.; Lelong, D.; Rosanski, W.; Cieplak, P., *Phys Chem Chem Phys* **2010**, *12* (28), 7821-39.
15. Vanquelef, E.; Simon, S.; Marquant, G.; Garcia, E.; Klimerak, G.; Delepine, J. C.; Cieplak, P.; Dupradeau, F. Y., *Nucleic Acids Res* **2011**, *39* (Web Server issue), W511-7.
16. Ryckaert, J. P. C., G.; Berendsen, H. J. C., *Journal of Computational Physics* **1977**, *23*, 327-341.
17. Gohlke, H.; Case, D. A., *J Comput Chem* **2004**, *25* (2), 238-50.
18. Kollman, P. A.; Massova, I.; Reyes, C.; Kuhn, B.; Huo, S.; Chong, L.; Lee, M.; Lee, T.; Duan, Y.; Wang, W.; Donini, O.; Cieplak, P.; Srinivasan, J.; Case, D. A.; Cheatham, T. E., 3rd, *Acc Chem Res* **2000**, *33* (12), 889-97.
19. Miller, B. R., 3rd; McGee, T. D., Jr.; Swails, J. M.; Homeyer, N.; Gohlke, H.; Roitberg, A. E., *J Chem Theory Comput* **2012**, *8* (9), 3314-21.
20. Srinivasan, J. C., T. E.; Cieplak, P.; Kollman, P. A.; Case, D. A., *Journal of the American Chemical Society* **1998**, (120), 9401-9409.
21. Wang, C.; Nguyen, P. H.; Pham, K.; Huynh, D.; Le, T. B.; Wang, H.; Ren, P.; Luo, R., *J Comput Chem* **2016**, *37* (27), 2436-46.
22. Yang, T. Y. W., J. C.; Yan, C. L.; Wang, Y. F.; Luo, R.; Gonzales, M. B.; Dalby, K. N.; Ren, P. Y., *Proteins-Structure Function and Bioinformatics* **2011**, *79*, 1940-1951.
23. Wang, J.; Cai, Q.; Li, Z.-L.; Zhao, H.-K.; Luo, R., *Chemical Physics Letters* **2009**, *468* (4-6), 112-118.
24. Wang, J.; Luo, R., *Journal of Computational Chemistry* **2010**, *31* (8), 1689-1698.
25. Cai, Q.; Hsieh, M.-J.; Wang, J.; Luo, R., *Journal of Chemical Theory and Computation* **2010**, *6* (1), 203-211.
26. Wang, J.; Cai, Q.; Xiang, Y.; Luo, R., *Journal of Chemical Theory and Computation* **2012**, *8* (8), 2741-2751.
27. Botello-Smith, W. M.; Luo, R., *J Chem Inf Model* **2015**, *55* (10), 2187-99.

28. Tan, C.; Tan, Y.-H.; Luo, R., *Journal of Physical Chemistry B* **2007**, *111* (42), 12263-12274.
29. Galindo-Murillo, R.; Roe, D. R.; Cheatham, T. E., 3rd, *Biochim Biophys Acta* **2015**, *1850* (5), 1041-58.
30. de Beer, T. A.; Berka, K.; Thornton, J. M.; Laskowski, R. A., *Nucleic Acids Res* **2014**, *42* (Database issue), D292-6.
31. Laskowski, R. A., *Nucleic Acids Res* **2001**, *29* (1), 221-2.
32. Laskowski, R. A.; Hutchinson, E. G.; Michie, A. D.; Wallace, A. C.; Jones, M. L.; Thornton, J. M., *Trends Biochem Sci* **1997**, *22* (12), 488-90.

## SI Tables

**Table S1. Statistics of Data Collection, Processing and Refinement**

	prop-DpsC + 1
<b>Data collection</b>	
Wavelength (Å)	1.0
Total reflections	85634 (7822)
Unique reflections	43341 (4164)
Space group	P 6 <sub>5</sub> 2 2
Cell dimensions	
<i>a</i> , <i>b</i> , <i>c</i> (Å)	91.6, 91.6, 316.1
$\alpha$ , $\beta$ , $\gamma$ (°)	90, 90, 120
Resolution (Å)	70.9 – 2.15
<i>R</i> <sub>merge</sub>	0.021 (0.134)
<i>R</i> <sub>meas</sub>	0.030 (0.190)
<i>I</i> / $\sigma$ ( <i>I</i> )	16.26 (4.26)
<i>CC</i> <sub>1/2</sub>	0.999 (0.978)
<i>CC</i> *	1.0 (0.994)
Completeness (%)	99 (95)
Redundancy	2.0 (1.9)
Wilson B-factor	35.15
<b>Refinement</b>	
Resolution (Å)	70.9 – 2.15
No. reflections	43233 (4160)
<i>R</i> <sub>work</sub>	0.179
<i>R</i> <sub>free</sub>	0.209
No. atoms	
Protein	5083
Ligands	60
<i>B</i> factors	
Protein	39.56
Ligands	95.06
Water	44.86
Ramachandran	

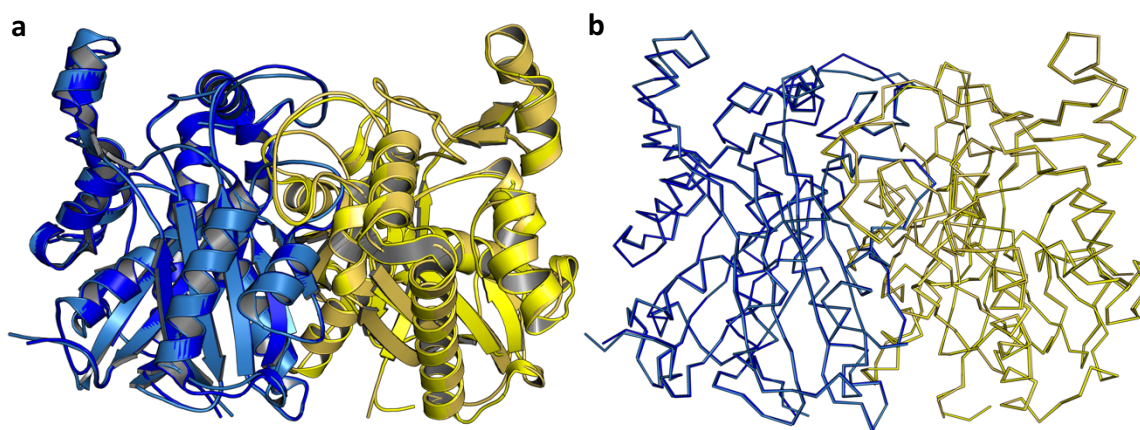
**Table S2.** DpsC & Ligand Simulation Conditions

<b>Simulation Number</b>	<b>System</b>	<b>Temperature (K)</b>	<b>Time (ns)</b>	<b>Traj. Num.</b>	<b>Ions</b>	<b>Waters</b>
1	DpsC & malonate-based <b>1</b>	310	100	1	16 Na <sup>+</sup>	14,767
2	DpsC & malonate-based <b>1</b>	310	100	1	16 Na <sup>+</sup>	14,767
3	DpsC & malonate-based <b>1</b>	310	100	1	16 Na <sup>+</sup>	14,767
4	DpsC & oxetane-based <b>1</b>	310	100	1	16 Na <sup>+</sup>	14,769
5	DpsC & oxetane-based <b>1</b>	310	100	1	16 Na <sup>+</sup>	14,769
6	DpsC & oxetane-based <b>1</b>	310	100	1	16 Na <sup>+</sup>	14,769

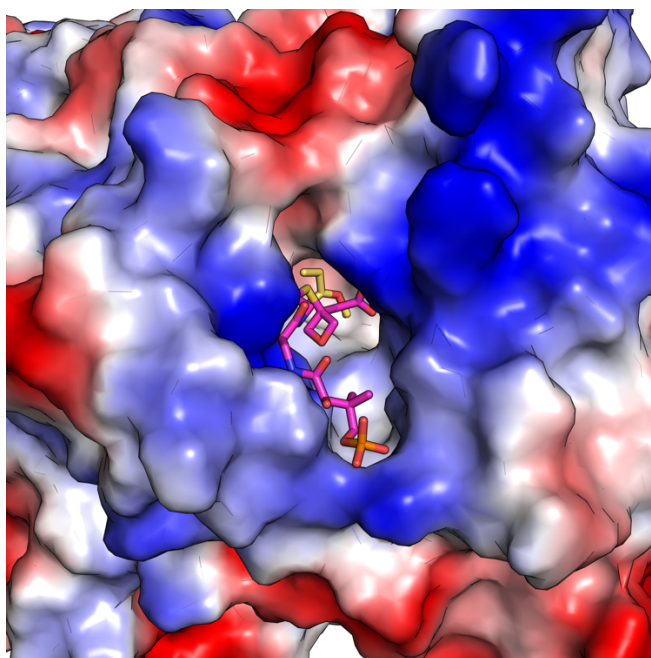
**Table S3.** MM/PBSA-derived  $\Delta G$  Relative Binding Free Energy Approximations (kcal/mol)

<b>Simulation Number</b>	<b>DpsC Chain &amp; Ligand</b>	<b><math>\Delta G</math></b>	<b>Standard Deviation</b>	<b>Standard Error</b>
1	DpsC Chain B & malonate-based <b>1</b>	-16.83	4.54	0.144
2	DpsC Chain B & malonate-based <b>1</b>	-16.00	4.14	0.131
3	DpsC Chain B & malonate-based <b>1</b>	-13.43	4.32	0.137
4	DpsC Chain B & oxetane-based <b>1</b>	-15.36	3.68	0.117
5	DpsC Chain B & oxetane-based <b>1</b>	-15.11	4.03	0.128
6	DpsC Chain B & oxetane-based <b>1</b>	-15.45	3.70	0.117

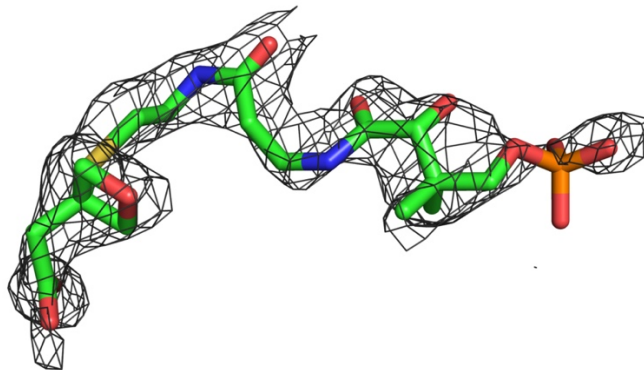
## SI Figures



**Figure S1.** Ligand-free and ligand-bound structural comparison. **a**, the ligand-free structure of prop-DpsC (dark blue and bright yellow) is overlaid with the ligand-bound structure (light blue and pale yellow) in cartoon representation. **b**, the ligand-free structure of prop-DpsC (dark blue and bright yellow) is overlaid with the ligand-bound structure (light blue and pale yellow) in ribbon representation.

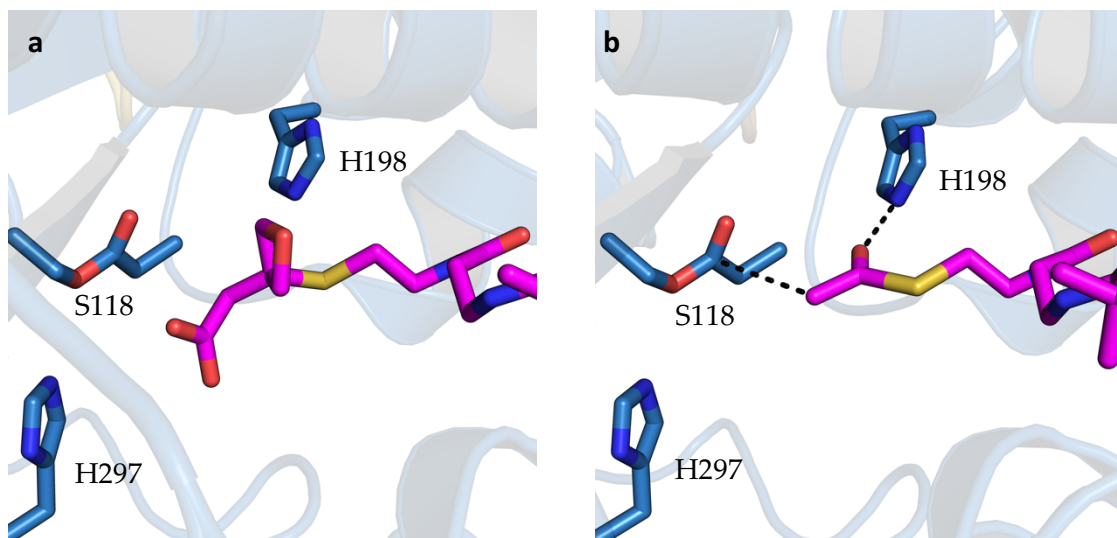


**Figure S2.** DpsC active site pocket. The surface of DpsC is represented as surface electrostatics. **1** is shown in magenta sticks, and the propionylated S118 sidechain is shown in yellow sticks.

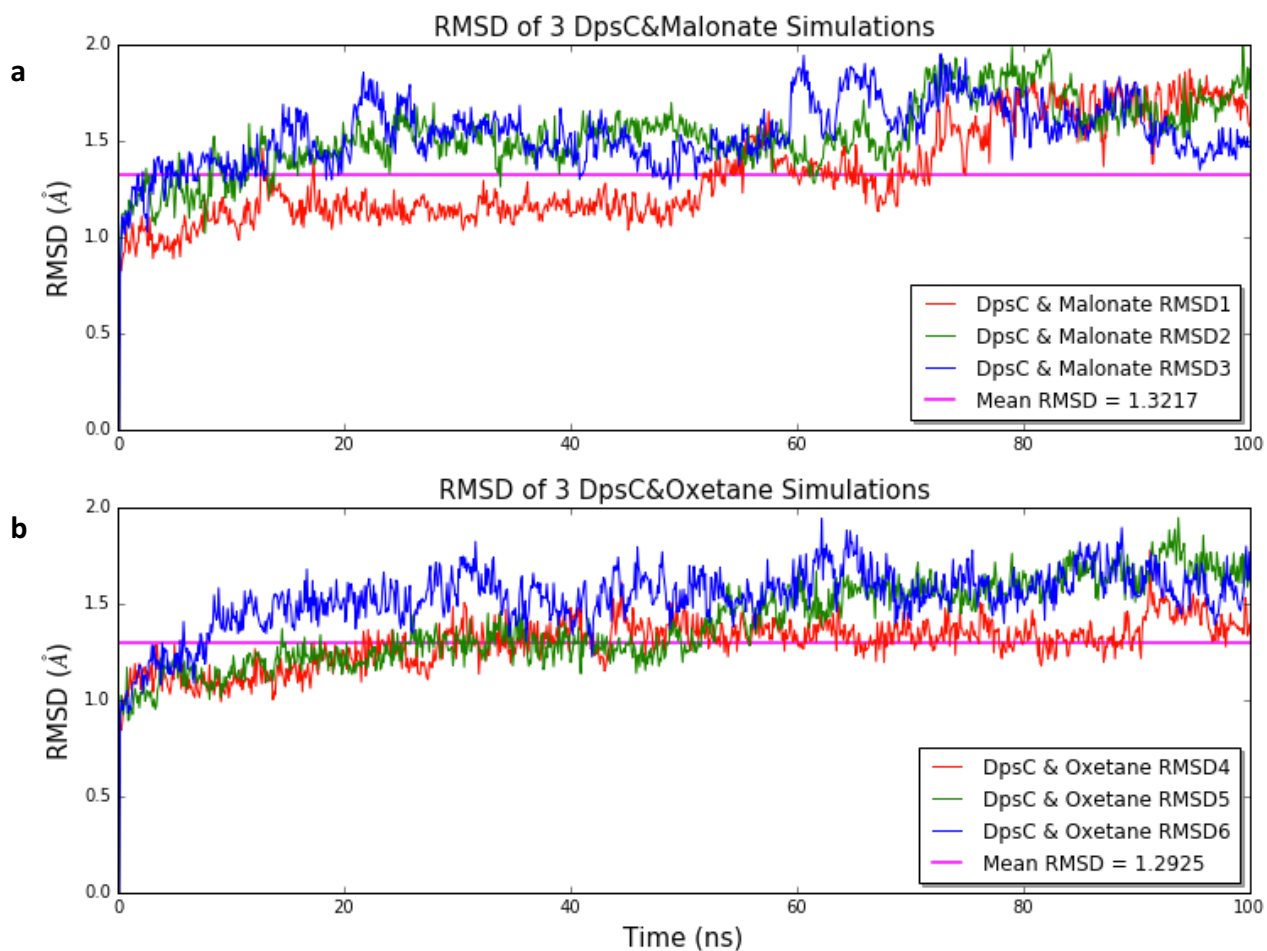


**Figure S3.** SA-Omit  $|2F_o - F_c|$  map for **1** contoured at 0.8 sigma.

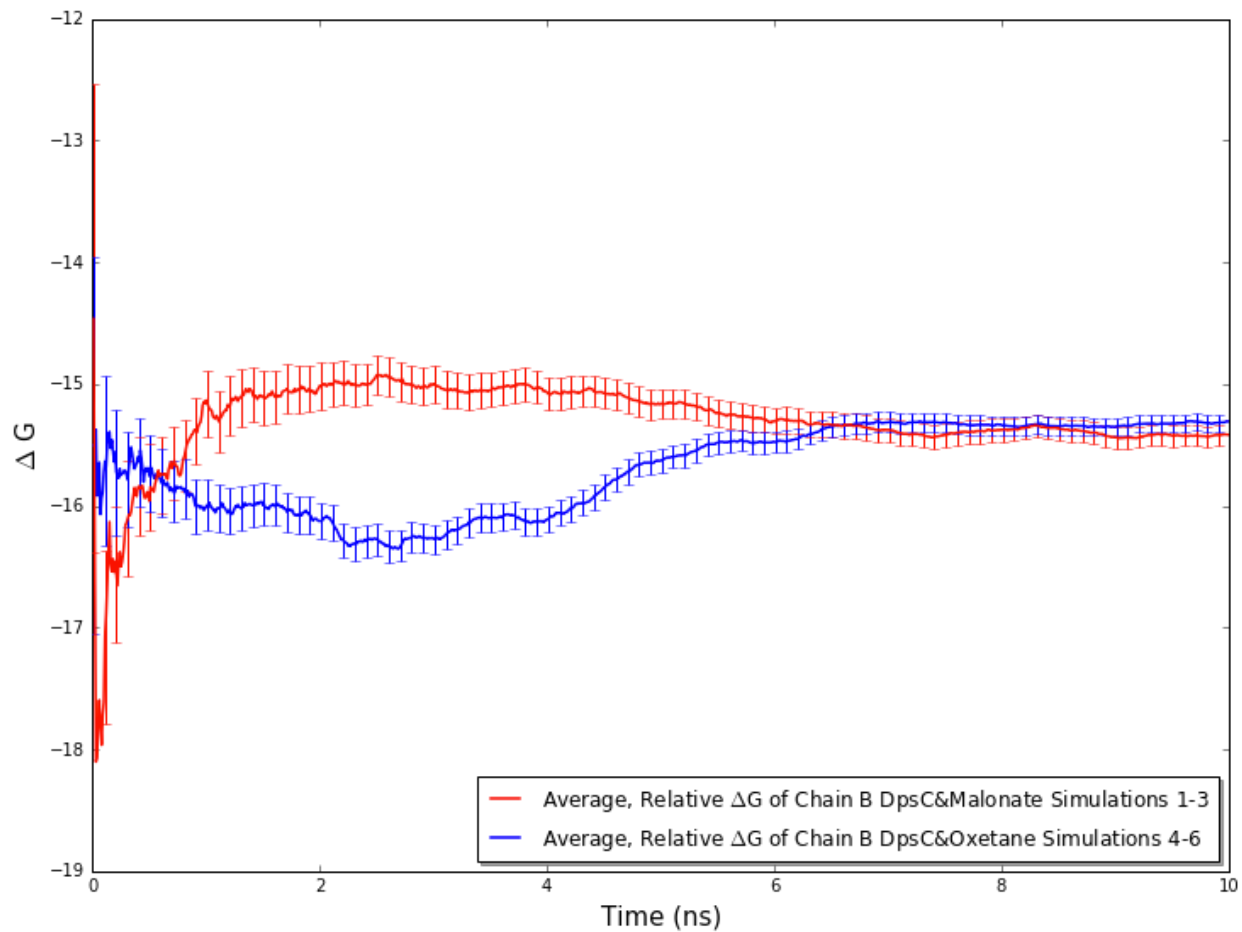




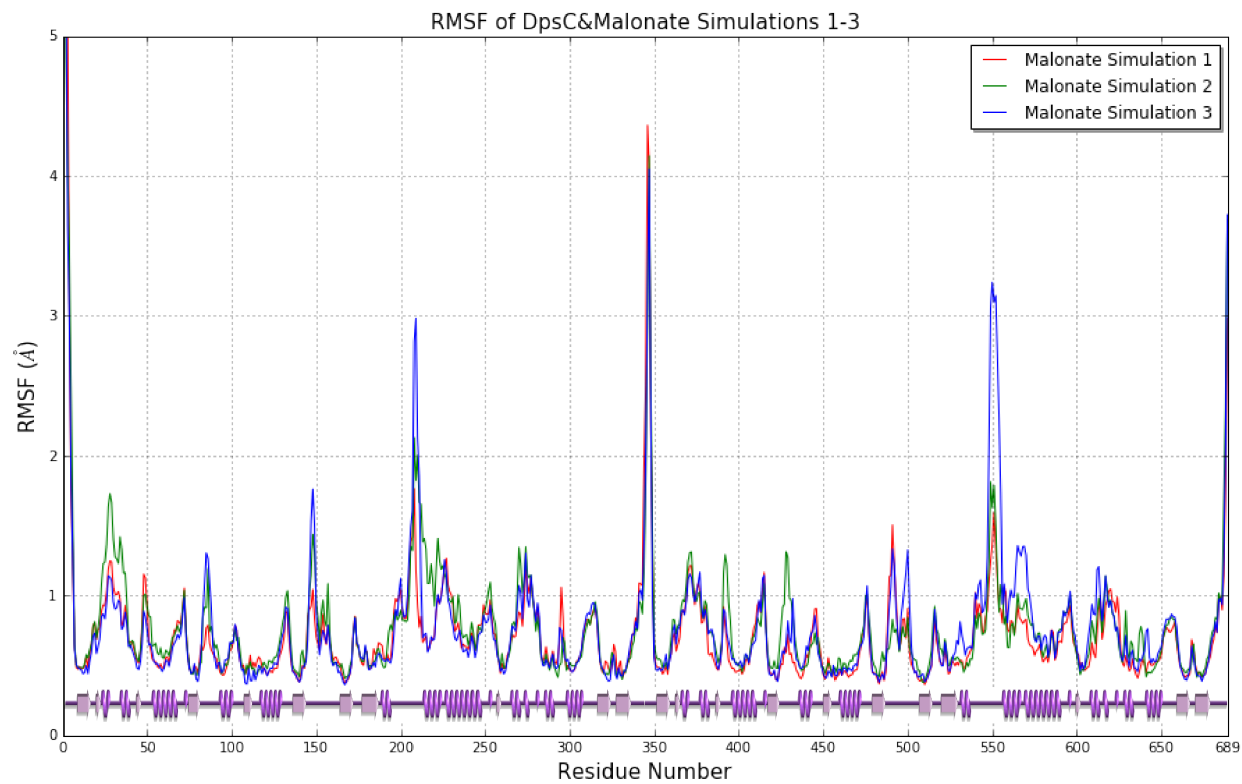
**Figure S4.** Proposed DpsC oxyanion hole. **a**, crystal structure of prop-DpsC with **1**, showing the putative oxyanion hole residue H198. **b**, a proposed model showing a post-decarboxylation substrate that has rotated to interact with H198.



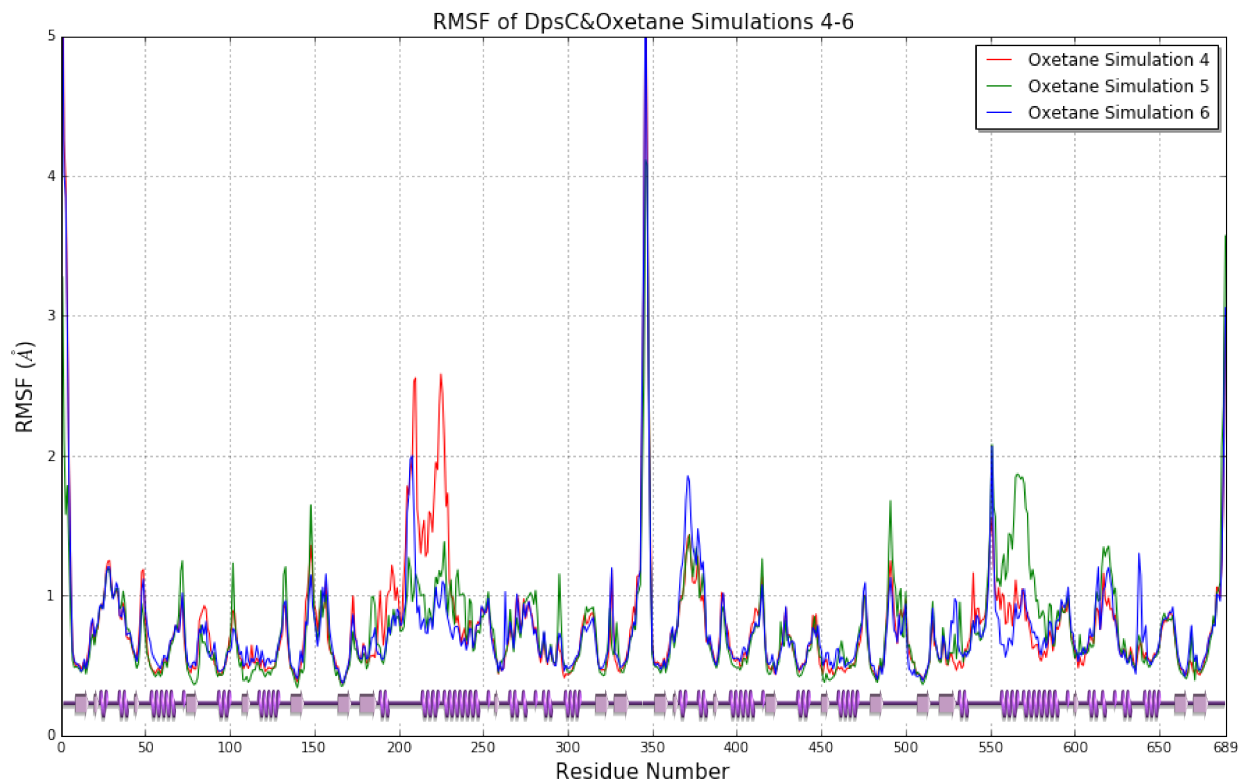
**Figure S5.** Backbone (C, C $\alpha$ , N, O) RMSD of 100-ns, DpsC-malonate simulations 1-3 and DpsC-oxetane simulations 4-6. **a**, all DpsC-malonate simulations converge within 100-ns, averaging to 1.322 Å. **b**, all DpsC-oxetane simulations converge within 100-ns, averaging to 1.292 Å.



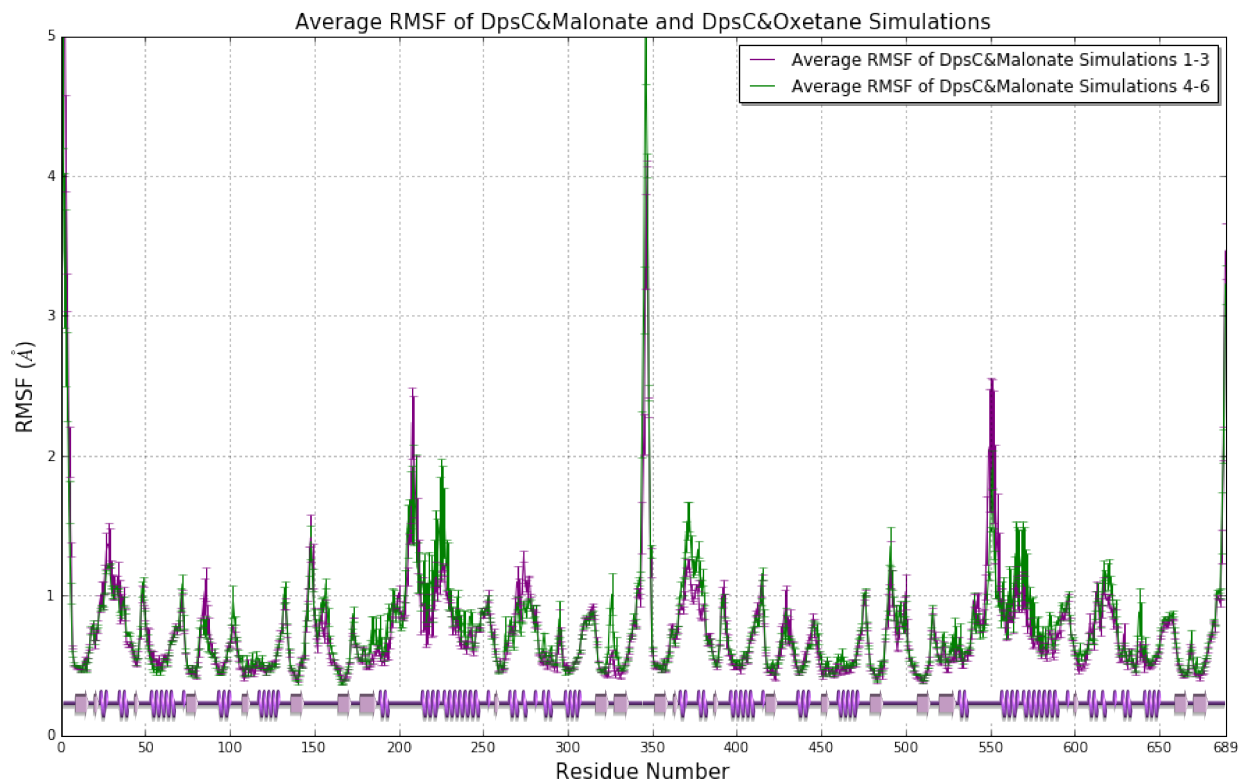
**Figure S6.** Convergence trend lines of average  $\Delta G$  binding energy calculations of DpsC-malonate simulations 1-3 and DpsC-oxetane simulations 4-6. The malonate-bound average  $\Delta G$  converges to -44.50 kcal/mol after 7 ns, and oxetane-bound average  $\Delta G$  converges to -45.80 kcal/mol after 7 ns.



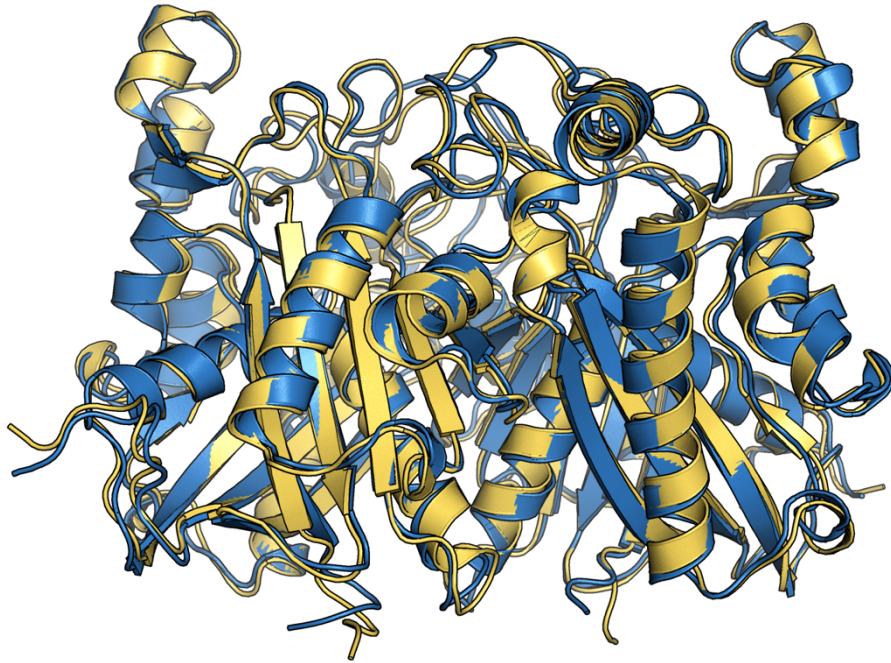
**Figure S7.** Heavy-atom (C, C $\alpha$ , N, O) RMSF of all DpsC-malonate simulations. Secondary structure is depicted using PDBsum-generated imaging adjacent to the x-axis<sup>30-32</sup>.



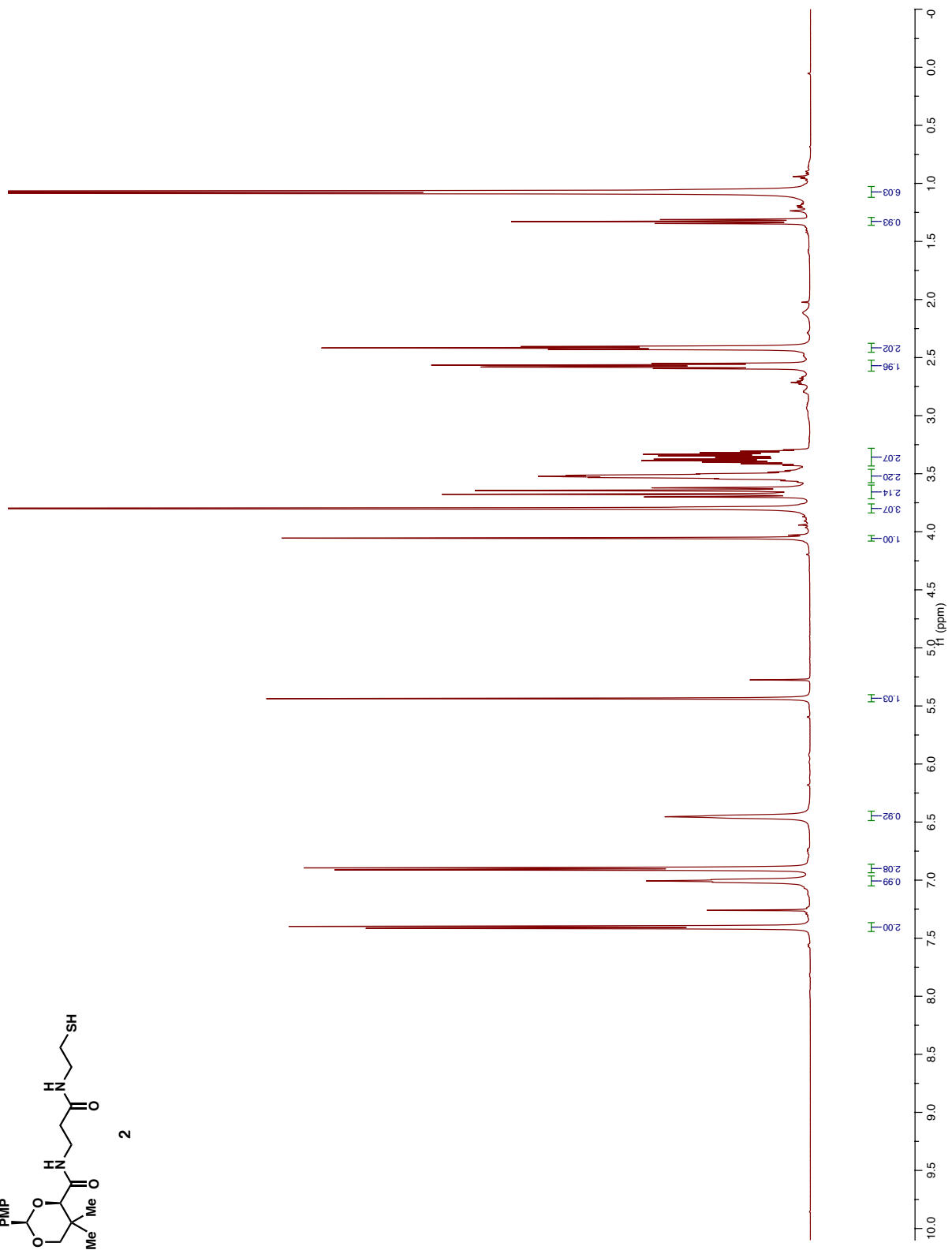
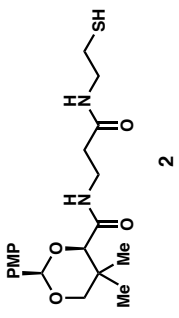
**Figure S8.** Heavy-atom (C, C $\alpha$ , N, O) RMSF of all DpsC-oxetane simulations. Secondary structure is depicted using PDBsum-generated imaging adjacent to the x-axis<sup>30-32</sup>.



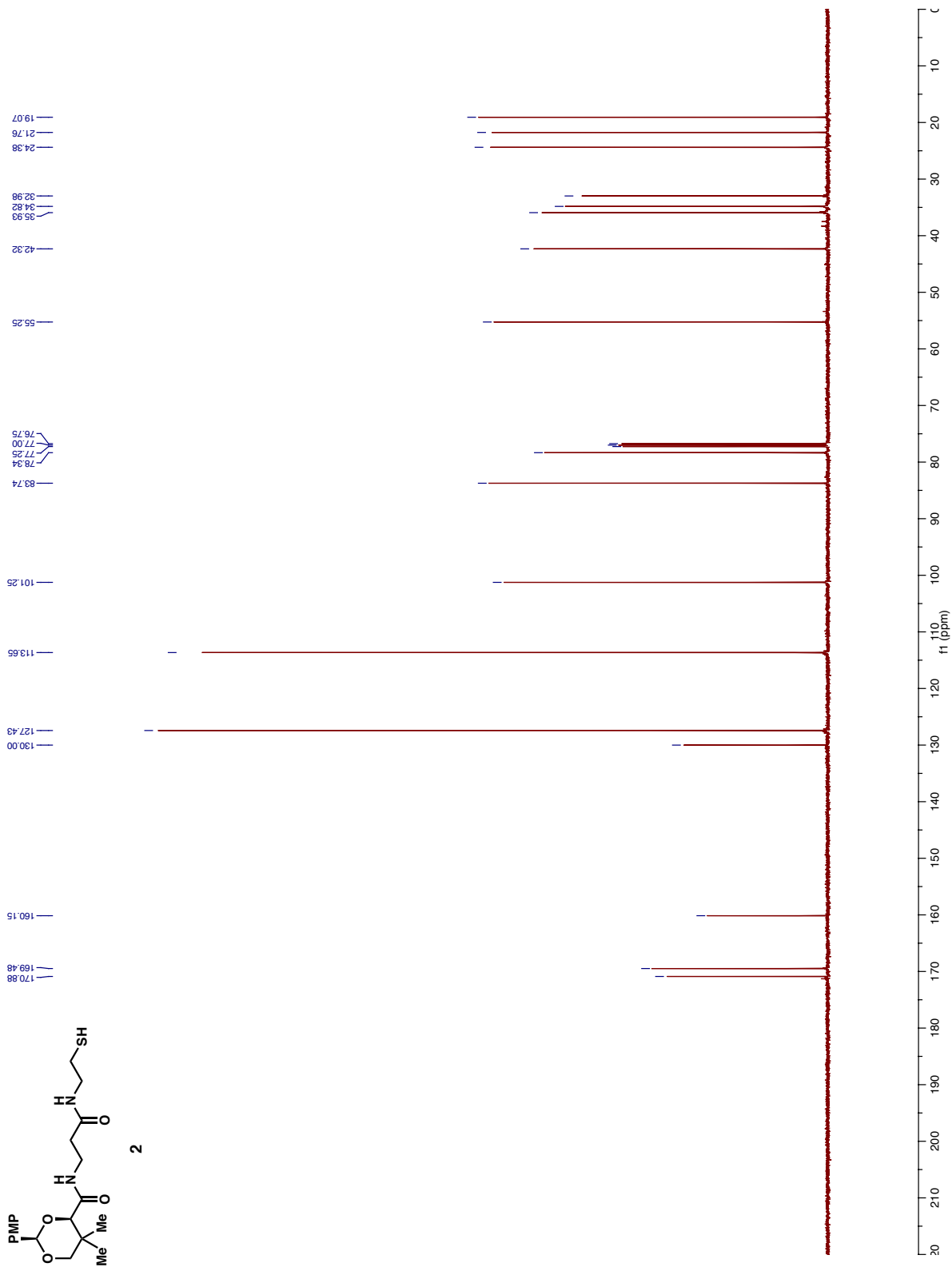
**Figure S9.** Average backbone (C, C $\alpha$ , N, O) RMSF of all DpsC-malonate and DpsC-oxetane simulations. Secondary structure is depicted using PDBsum-generated imaging adjacent to the x-axis<sup>30-32</sup>.

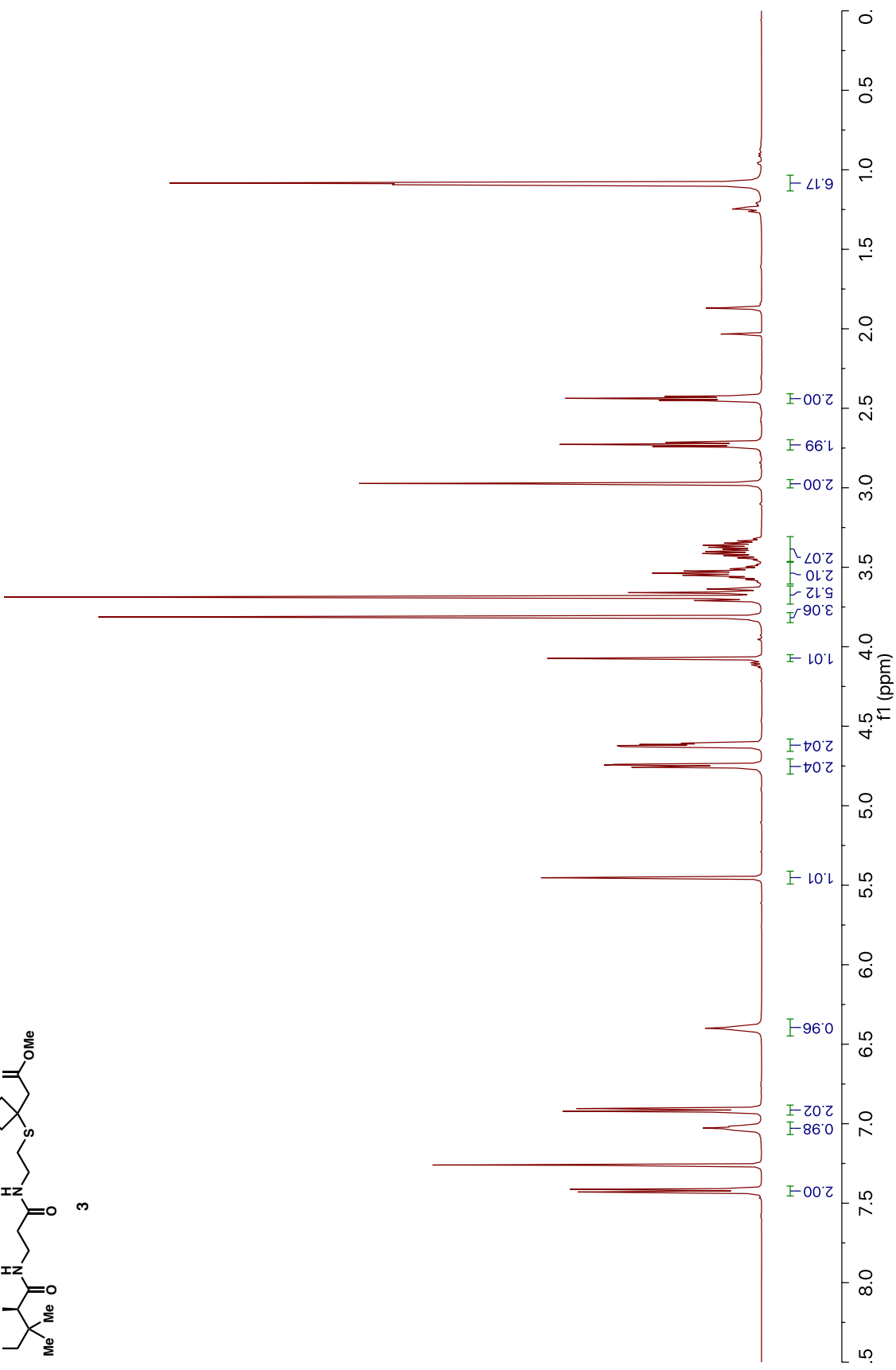
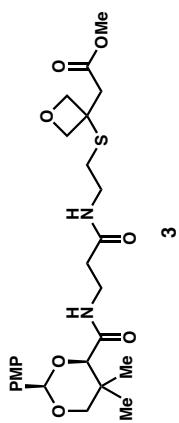


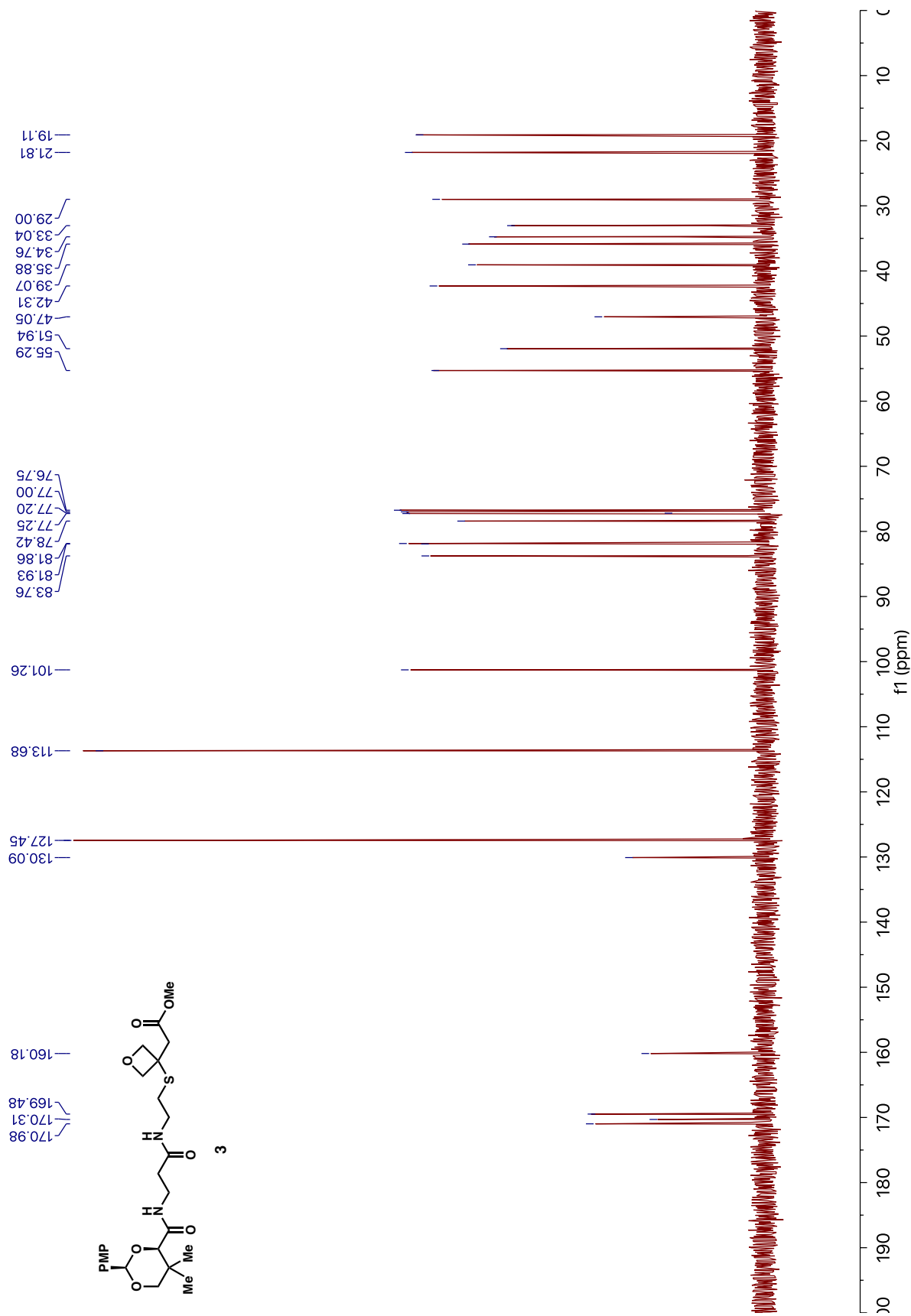
**Figure S10.** Alignment of mean structures from DpsC-malonate simulations (yellow) and DpsC-oxetane simulations (blue). Backbone RMSD is 0.716Å after alignment.

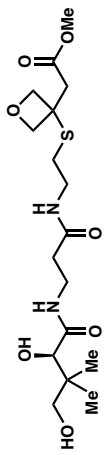




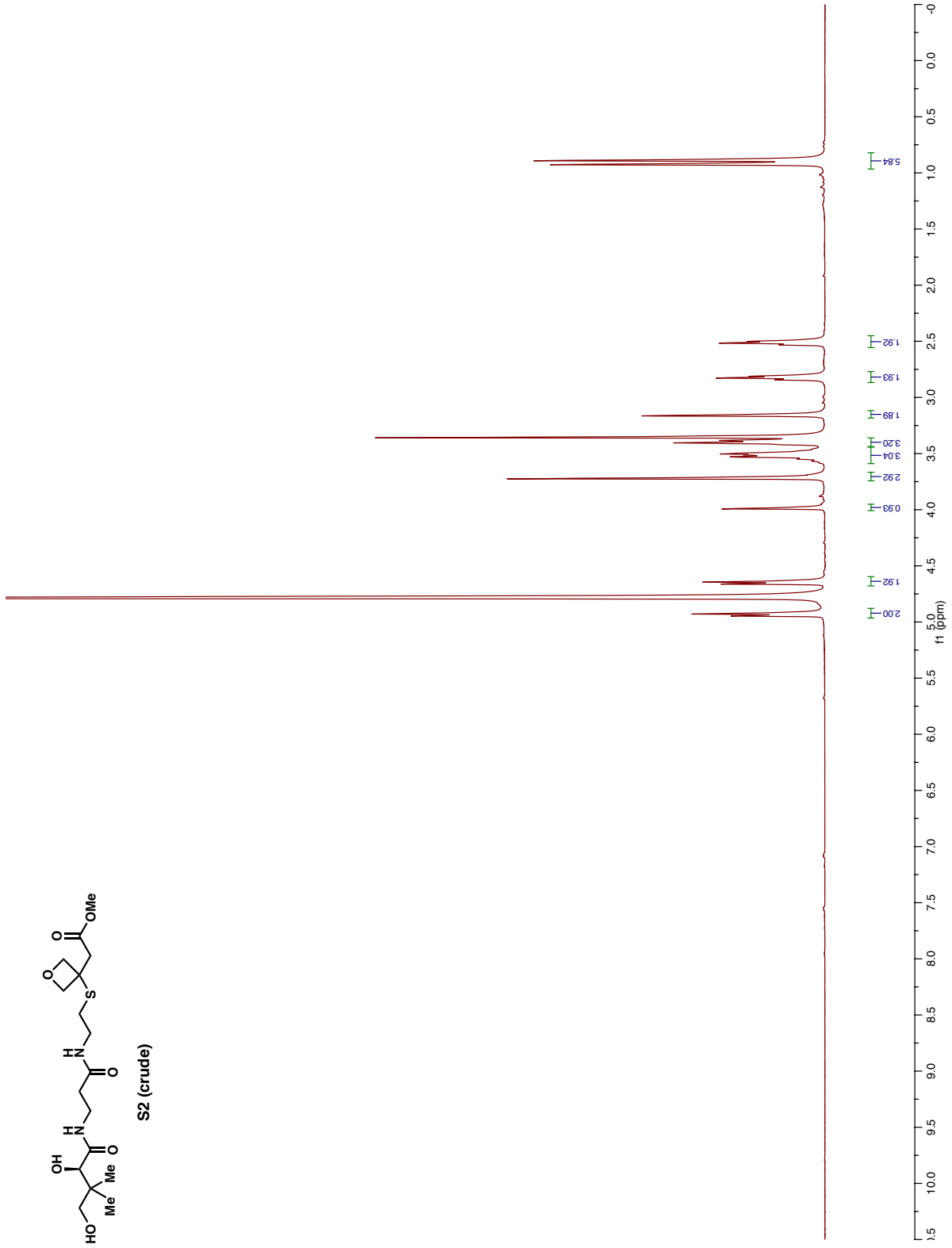


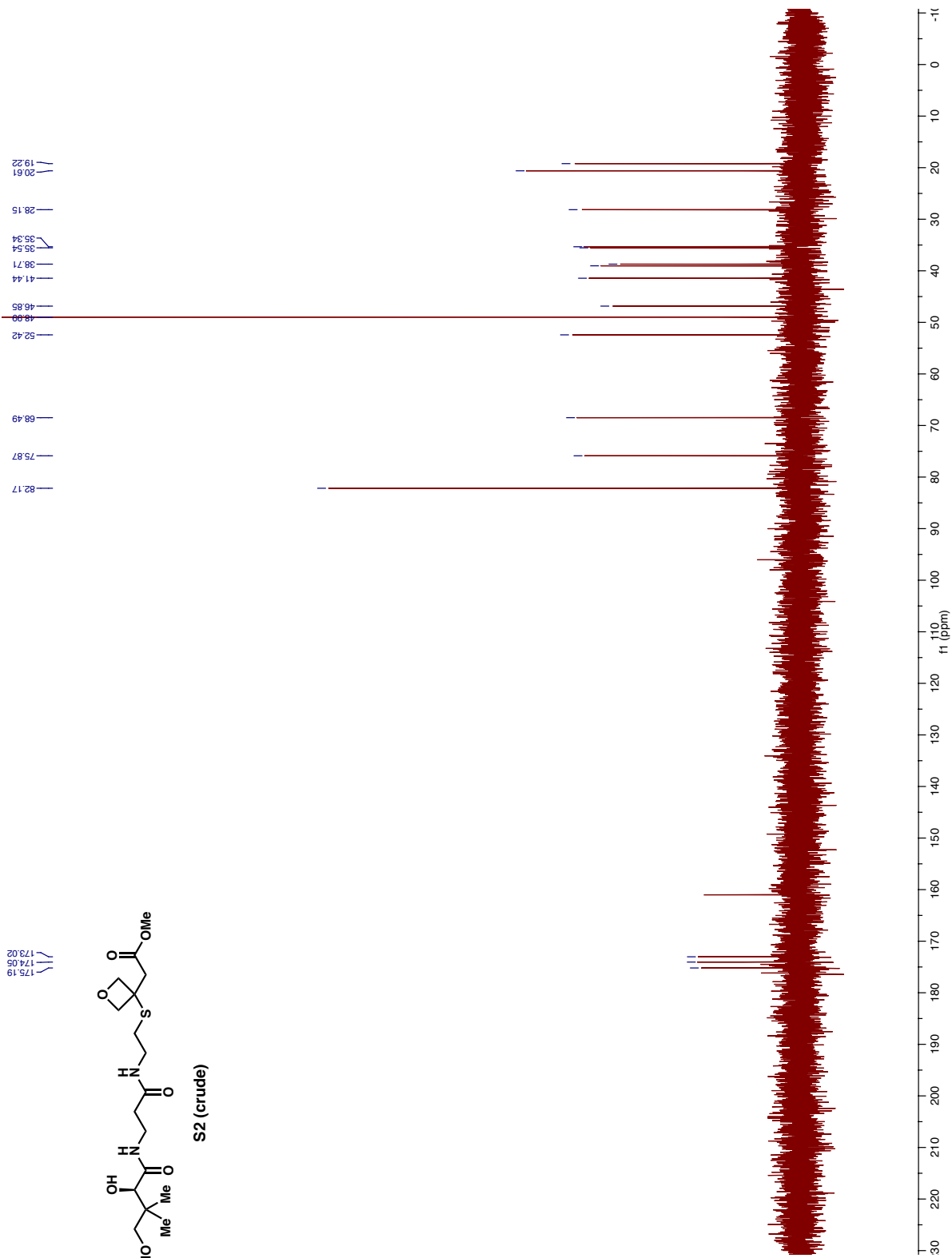


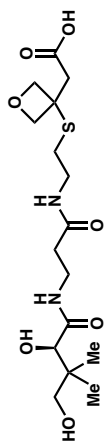




S2 (crude)







4 (crude)

